Chemical Vapor Deposition of Niobium Disulfide Thin Films

Claire J. Carmalt,*[a] Emily S. Peters,[a] Ivan P. Parkin,[a] Troy D. Manning,[a] and Andrew L. Hector[b]

Keywords: Niobium disulfide / Thin films / Chemical vapor deposition

Atmospheric pressure chemical vapor deposition (APCVD) of niobium sulfide coatings was achieved on glass substrates from the reaction of $NbCl_5$ and $S(SiMe_3)_2$, tBu_2S_2, *t*BuSH, or $HSCH_2CH_2SH$ at 250–600 °C. The niobium sulfide films grown at temperatures above 500 °C were crystalline, and powder X-ray diffraction showed that two polytypes of NbS_2 were produced. The sulfur precursor used is fundamental to the polytype of NbS_2 obtained; films that are grown from the APCVD reaction of $NbCl_5$ and $S(SiMe_3)_2$ or tBu_2S_2 at 500–600 °C crystallize into the 1T structure, whereas those grown from the APCVD reaction of $NbCl_5$ and *t*BuSH or $HSCH_2CH_2SH$ at 500–600 °C crystallize into the 3R structure. Energy dispersive X-ray analysis (EDXA) studies gave elemental ratios close to the expected 1:2 ratio for Nb:S. Scanning electron microscopy (SEM) revealed surface morphologies consistent with an island growth mechanism. The films were also characterized using Raman and X-ray photoelectron spectroscopy, both of which showed differences consistent with the formation of the two polytypes, 1T and 3R-NbS_2.

Introduction

Niobium sulfides are part of the family of transition metal dichalcogenide layered materials, which gives rise to a host of interesting properties and facilitates intercalation into the van der Waals gap between these layers.[1] This function of transition metal dichalcogenides has been exploited for use as the cathode material in secondary batteries.[1] The layer structure also gives rise to unique optical and magnetic properties, which have been widely studied.[2−4] Niobium disulfide (NbS_2) has found uses as hydrodesulfurization and hydrodenitrogenation catalysts for hydrotreatment reactions in the purification of petroleum.[5] In addition, NbS_2 has been shown to be an effective humidity sensor.[6] However, the development of new applications has been hampered by difficulty in forming thin-films of NbS_2.

There are two known phases of NbS_2, termed 2H and 3R, both of which can also form nonstoichiometric phases with $Nb_{1+x}S_2$ compositions.[7,8] 2H-NbS_2 is a superconductor with a transition range of 5−6.3 K, whereas 3R-NbS_2 has a superconducting transition temperature of 1.7 K.[9,10] The stoichiometry of the niobium sulfide obtained is very sensitive to pressure, making identification of the polytype difficult due to the formation of substoichiometric compounds and mixtures.[9] The formation of niobium sulfides with high surface areas, such as in thin-film form, is particularly important in battery, gas sensing and catalyst applications.[1,5,10] However, there have been relatively few reports on thin-film formation of NbS_2, a possible consequence of the difficulty in isolating a single polytype.[11,12] Physical deposition processes for the preparation of NbS_2 films have been reported.[11] However, chemical vapor deposition (CVD) routes to niobium sulfide films are limited and involve the use of the single-source precursors $[NbCl_4(S_2\text{-}i\text{Pr}_2)][NbCl_6]$[12] and $[Nb(S\text{-}2,6\text{-}Me_2C_6H_3)_5]$,[13] resulting in thin-films of Nb_2O_5/NbS_2 and NbS, respectively.

In this paper we report the atmospheric pressure (AP)CVD reaction of $NbCl_5$ with $S(SiMe_3)_2$, tBu_2S_2, *t*BuSH or $HSCH_2CH_2SH$. The formation of a new trigonal polytype 1T-NbS_2 is described and the effect of the sulfur precursor on the phase of the NbS_2 film formed is discussed.[14]

Results and Discussion

Films have been deposited on glass from the dual source APCVD reaction of $NbCl_5$ with a range of sulfur sources [$S(SiMe_3)_2$, tBu_2S_2, *t*BuSH and $HSCH_2CH_2SH$]. The onset of deposition varied from 250−600 °C, a consequence of the sulfur-bonding environment in the precursor [onset of deposition: $S(SiMe_3)_2$ 600 °C; tBu_2S_2 400 °C; *t*BuSH 250 °C; $HSCH_2CH_2SH$ 350 °C]. At temperatures above 500 °C, deposition was localized towards the front of the substrate, at lower temperatures complete coverage was observed. The

[a] Department of Chemistry, Christopher Ingold Laboratories, University College London,
London, WC1H OAJ, UK
Fax: (internat.) + 44-2076797463
E-mail: c.j.carmalt@ucl.ac.uk
[b] School of Chemistry, University of Southampton,
Highfield, Southampton, SO17 1BJ, UK

  DOI: 10.1002/ejic.200400308

films produced from $NbCl_5$ and $S(SiMe_3)_2$ or tBu_2S_2 at 500 °C or above had a gold color, and the lower temperature (< 500 °C) films were reflective. The reflectance and transmission spectra indicate that all the films have good reflectance and minimal transmission in the region 400−1000 nm. APCVD of $NbCl_5$ and *t*BuSH or $HSCH_2CH_2SH$ produced dark brown, reflective films at all temperatures. All the films produced, regardless of the sulfur precursor used or temperature of the reaction, were adhered to the substrate, passing the Scotch tape test. However, they were readily scratched by a brass or stainless steel stylus. The films were chemically robust to toluene, dichloromethane, THF and acetone, showing no visible changes after 2 weeks of immersion. Concentrated nitric acid digested the films within 1 min of immersion, whereas concentrated hydrochloric acid dissolved the films after 2 hours.

The niobium sulfide films were characterized by a range of techniques. Composition analysis of the films was determined by EDAX analysis, which shows niobium to sulfur ratios close to the expected 1:2 for NbS_2 (Table 1). Some slight deviations from this composition were noted; however, this tended to be for thinner films where breakthrough to the underlying glass was observed, which interfered with accurate compositional analysis. No evidence of carbon or chlorine contamination was found, within the detection limit of the instrument (1 atom%). Interestingly, the films produced from $NbCl_5$ and $HSCH_2CH_2SH$ at 350−400 °C were slightly rich in sulfur (Table 1). Scanning electron microscopy (SEM) shows that each film grew by a Volmer−Webber type growth mechanism. However the morphology of the films varied depending on the sulfur precursor employed in the APCVD reaction (Figure 1).

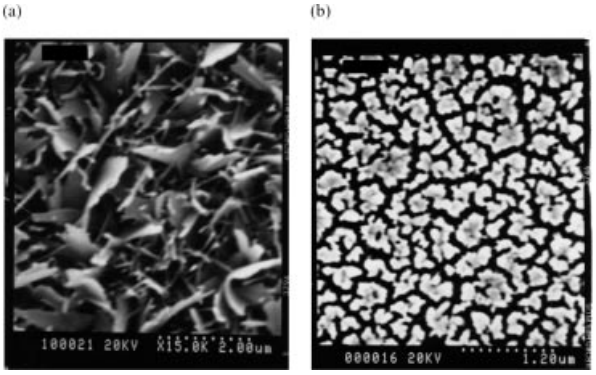

Figure 1. Scanning electron microscopy image of the film prepared from (a) APCVD of $NbCl_5$ and tBu_2S_2 at 550 °C and (b) APCVD of $NbCl_5$ and $HSCH_2CH_2SH$ at 550 °C

SEM of the films grown from $NbCl_5$ and $S(SiMe_3)_2$ or tBu_2S_2 show platelets (approximately 2 μm at 550 °C) that are orientated largely perpendicular to the substrate (Figure 1, a). In contrast, SEM of films produced from $NbCl_5$ and *t*BuSH or $HSCH_2CH_2SH$ display a crazy paving type morphology with particle sizes of 0.6 μm at 550 °C (Figure 1, b) and 0.25 μm at 400 °C. Edge-on SEM photographs allowed for the determination of film thickness. For example, films grown at 600 °C from $NbCl_5/S(SiMe_3)_2$ or tBu_2S_2 were 16 μm thick, whereas films from $NbCl_5/t$BuSH or $HSCH_2CH_2SH$ (at the same growth temperature) were

Table 1. Deposition conditions and analysis of the films grown from the APCVD of $NbCl_5$ and $S(SiMe_3)_2$, tBu_2S_2, *t*BuSH or $HSCH_2CH_2SH$

Substrate temp. (°C); sulfur precursor	Deposition time (min)	EDXA	Raman (cm^{-1})	XRD / 2θ	Contact angle (°)
600; $S(SiMe_3)_2$	5	$NbS_{1.8}$	1T-NbS_2	1T-NbS_2	95.1
600; tBu_2S_2	5	$NbS_{1.9}$	1T-NbS_2	1T-NbS_2	6.0
550; tBu_2S_2	5	$NbS_{1.8}$	1T-NbS_2	1T-NbS_2	3.5
500; tBu_2S_2	5	$NbS_{2.1}$	1T-NbS_2	1T-NbS_2	9.2
450; tBu_2S_2	5	$NbS_{2.1}$	90, 224, 285, 417, 604, 924	–[a]	87.3
400; tBu_2S_2	5	$NbS_{1.7}$	93, 226, 282, 418, 605, 924	–[a]	8.4
600; *t*BuSH	5	$NbS_{1.6}$	3R-NbS_2	3R-NbS_2	3.2
550; *t*BuSH	5	$NbS_{1.7}$	3R-NbS_2	3R-NbS_2	3.1
500; *t*BuSH	5	$NbS_{1.7}$	3R-NbS_2	3R-NbS_2	3.5
450; *t*BuSH	5	$NbS_{1.9}$	3R-NbS_2	3R-NbS_2	4.8
400; *t*BuSH	5	$NbS_{1.7}$	3R-NbS_2	3R-NbS_2	2.4
350; *t*BuSH	5	$NbS_{2.0}$	3R-NbS_2	3R-NbS_2	4.1
300; *t*BuSH	5	$NbS_{2.0}$	169, 241, 372	X-ray amorphous	4.1
250; *t*BuSH	5	$NbS_{2.0}$	187, 294, 328, 549	X-ray amorphous	14.5
600; $HSCH_2CH_2SH$	5	$NbS_{2.1}$	3R-NbS_2	3R-NbS_2	54
550; $HSCH_2CH_2SH$	5	$NbS_{1.2}$	3R-NbS_2	3R-NbS_2	87
500; $HSCH_2CH_2SH$	5	$NbS_{1.8}$	3R-NbS_2	3R-NbS_2	90
500; $HSCH_2CH_2SH$	4	$NbS_{1.9}$	3R-NbS_2	X-ray amorphous	105
500; $HSCH_2CH_2SH$	3	$NbS_{1.8}$	195, 260, 328, 383	X-ray amorphous	48
450; $HSCH_2CH_2SH$	5	$NbS_{2.0}$	186, 260, 331, 381, 535	Nanocrystalline NbS_2	95
400; $HSCH_2CH_2SH$	5	$NbS_{2.4}$	197, 239, 299, 334, 535	X-ray amorphous	95
350; $HSCH_2CH_2SH$	5	$NbS_{2.3}$	187, 242, 298, 332, 544	X-ray amorphous	21

[a] Film too thin.

0.4 μm thick. This indicated that typical growth rates were 3.2 μm·min^{-1} [$NbCl_5$/$S(SiMe_3)_2$ or tBu_2S_2] and 0.1 μm·min^{-1} ($NbCl_5$/*t*BuSH or $HSCH_2CH_2SH$).

The niobium sulfide films grown at 500−600 °C (from $NbCl_5$ and $S(SiMe_3)_2$, tBu_2S_2 or $HSCH_2CH_2SH$) or 350−600 °C (from $NbCl_5$/*t*BuSH) were crystalline (Table 1). NbS_2 is known to form with two structure types, which have been classified as 3R and 2H. However, powder X-ray diffraction (XRD) of the crystalline films shows that two different polytypes of NbS_2 are produced (3R- and 1T-NbS_2), as shown in Scheme 1.

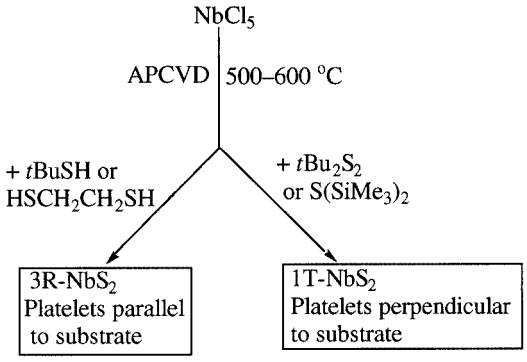

Scheme 1

Thus, films grown from $NbCl_5$/*t*BuSH or $HSCH_2CH_2SH$ formed nanocrystalline 3R-NbS_2, whereas $NbCl_5$/$S(SiMe_3)_2$ or tBu_2S_2 gave crystalline 1T-NbS_2. The XRD patterns for the nanocrystalline 3R-NbS_2 films formed from $NbCl_5$/*t*BuSH or $HSCH_2CH_2SH$ are shown in Figure 2.

The XRD patterns obtained for films that were grown from $NbCl_5$/$S(SiMe_3)_2$ or tBu_2S_2 at 600 °C indicate that the 3R-NbS_2 structure does not match the data well. Although the 2H-NbS_2 structure gives a similar diffraction pattern to the observed data, the 1T structure, as adopted by some other transition metal dichalcogenides (e.g. TaS_2),[7,15] is also a close match. The 2H structure comprises close packed sulfur atoms with an AABB repeating unit, with Nb located in half of the trigonal prismatic sites. The double layer repeating unit is shown in Figure 3, the structure in the *xy* plane shows edge-linked NbS_2 trigonal prisms. In contrast, the 1T structure consists of hexagonal close packed sulfur atoms (AB repeat unit) with Nb filling half of the octahedral holes in every other layer. Hence the structure shows edge-linked NbS_2 octahedra, two layers of the repeating unit are shown in Figure 3.

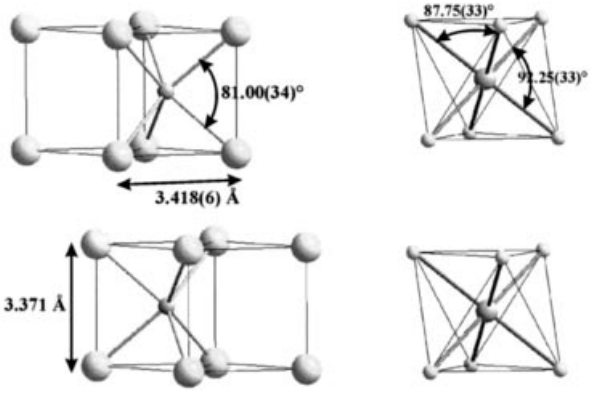

Figure 3. 2H (left) and 1T (right) NbS_2 structures; distances and angles shown are as refined from the NbS_2 thin films by XRD; thermal ellipsoids are shown at the 50% probability level

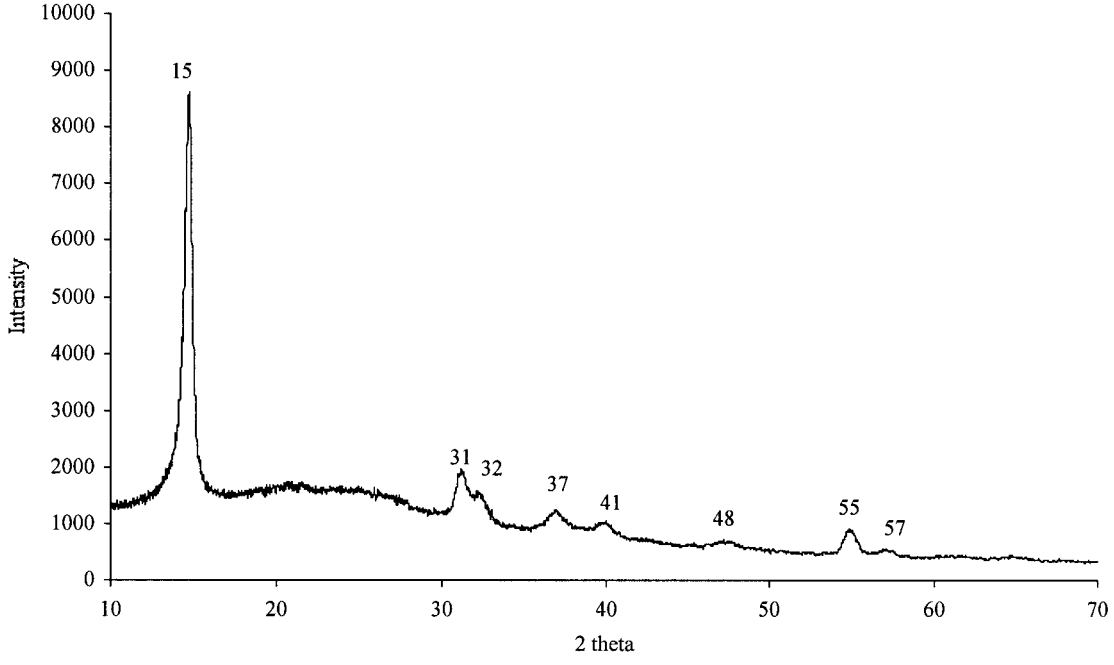

Figure 2. X-ray powder diffraction pattern for a 3R-NbS_2 film produced from the APCVD reaction of $NbCl_5$ and *t*BuSH at 550 °C

Rietveld refinements using the 2H and 1T structure models were performed with the GSAS package,[16] both were stable and converged. A cosine Fourier series (GSAS #2) with 6 terms was used to model the background and lattice parameters, zero point and scale factor were allowed to refine. Using profile function #2, the Gaussian terms were fixed at the values obtained with the Cu standard. The particle size broadening term was refined but no strain broadening was found. Transparency was also refined to a fairly high value (this is not surprising since the glass substrate was observed in the data, hence the offset in the tick marks on the fit diagrams). Particle size in Å is defined as $p = 18000\ K\lambda/\pi X$,[17] where K is the Scherrer constant and X is the particle size associated Lorentzian term from the Rietveld refinement. X is refined to 38 and 36 for the 2H and 1T structures, respectively, corresponding to an average crystallite size of around 180 Å. The preferred orientation ratio along 001 is refined to values of 1.18 (2H) and 1.27 (1T). Growth of the platelets perpendicular to the substrate is reflected in the apparent preferential *c*-axis growth in the diffraction data. The fit statistics are better for the 1T structure to a significant degree (Table 2). Furthermore, the 2H structure should have extra reflections, compared with the 1T structure, at 26.5° (101) and 32.5° (103) since it has a doubled *c* axis and these are not observed. The Nb thermal parameter in the 1T structure is slightly high but the S thermal parameter in the 2H structure is very high. The space group is $P\bar{3}m1$ (No. 164) and refined lattice parameters are $a = 3.420(6)$ Å and $c = 5.938(1)$ Å ($Z = 1$) (Figure 4). Prior to this work, there were no reports of NbS_2 crystallizing into the 1T structure.[14]

Table 2. Refined crystallographic parameters for NbS_2 with the 1T and 2H structure models.

	1T Structure	2H Structure
Space group	$P\bar{3}m1$ (No. 164)	$P6_3/mmc$ (No. 194)
Lattice constants *a*, *c* (Å)	3.420(6), 5.938(11)	3.418(6), 11.860(23)
Cell volume (Å^3)	60.16(19)	120.0(4)
Nb site	1a	2b
x, *y*, *z*	0, 0, 0	0, 0, $^1/_4$
U_{iso} (Å^2 × 100)	3.5(4)	2.4(3)
S site	2d	4f
x, *y*, *z*	$^1/_3$, $^2/_3$, 0.2491(29)	$^1/_3$, $^2/_3$, 0.1079(16)
U_{iso} (Å^2 × 100)	1.6(6)	7.8(7)
χ^2	1.893	2.363
R_{wp}	6.52%	7.29%
R_p	5.20%	5.67%
Nb–S (Å)	2.467(11)	2.595(13)
Nb–S–Nb (°)	87.8(5)	82.4(5)

Raman microscopy was used to investigate all of the films. The Raman spectra of the thin films that were grown from $NbCl_5$/*t*BuSH or $HSCH_2CH_2SH$ correspond well with that reported previously for 3R-NbS_2 [18] (Figure 5). Thus peaks at 322, 386, and 462 cm^{-1} are assigned to E_2, A_1 and A_2 modes, respectively. Other peaks were observed at approximately 190 and 258 cm^{-1}.

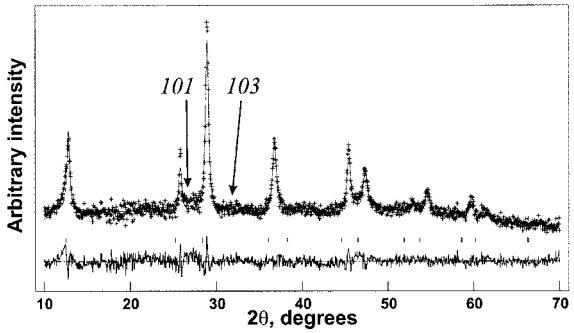

Figure 4. X-ray powder diffraction pattern for NbS_2 film produced from the APCVD reaction of $NbCl_5$ and tBu_2S_2 at 550 °C

It was noted that there was a slight shift in the Raman bands between samples that were sulfur-rich ($NbS_{2.3-2.4}$), fully stoichiometric (NbS_2) and sulfur-deficient ($NbS_{1.6-1.9}$). The formation of 1T-NbS_2 from $NbCl_5$/$S(SiMe_3)_2$ or tBu_2S_2 was further supported by the Raman spectra obtained for the films (Figure 6). It was found that the Raman spectra of the 1T-NbS_2 films is markedly different from those reported previously for 2H- and 3R-NbS_2,[18] but did show similarities with the 1T-TaS_2 pattern.[19]

X-ray photoelectron spectroscopy (XPS) shows that the surface of the films had been partially oxidized (depth of about 50 nm). The oxide surface layer was removed by sputtering to leave the bulk of the film consisting of niobium and sulfur. No evidence of chloride contamination (1–2% detection limit) was observed. XPS of films that were grown from $NbCl_5$ and *t*BuSH gave Nb $3d_{3/2}$, Nb $3d_{5/2}$, and S 2p binding energy shifts of 210.4, 207.5, and 162.3 eV, respectively. These are in good agreement with previous literature measurements for bulk NbS_2 (Nb $3d_{5/2}$ 207.7 eV).[20] XPS of the films that were grown from $NbCl_5$/$HSCH_2CH_2SH$ at temperatures > 400 °C also suggest the formation of 3R-NbS_2. However, XPS of films that were grown from $NbCl_5$/$HSCH_2CH_2SH$ at 350–400 °C show slight deviations (Nb $3d_{5/2}$ 207.4 eV, S 2p 162.3 eV) from the literature measurements of bulk NbS_2. As discussed above, the films that were grown from $NbCl_5$/$HSCH_2CH_2SH$ at 350–400 °C are shown by EDAX to be slightly sulfur-rich ($NbS_{2.3-2.4}$), which could result in shifts in the binding energies. Only one sulfur environment was found by XPS in all samples and this corresponds to the S^{2-} anion showing that these sulfur-rich samples are not a mixture of NbS_2 and NbS_3 (which would also contain the S_2^{2-} anion). It is also worth noting that $NbSe_2$ shows a phase change from 2H-$NbSe_2$ to 4H-$NbSe_2$ between 600–700 °C, which is slightly rich in selenium, 2H being the higher temperature phase.[21] Therefore, it is possible that a different phase to 3R-NbS_2 has been formed. Indeed, XPS of films that were grown from $NbCl_5$/$S(SiMe_3)_5$ or tBu_2S_2 at 500–600 °C gave Nb $3d_{3/2}$, Nb $3d_{5/2}$, and S 2p binding energy shifts of 209.4, 206.3, and 161.8 eV, respectively. The Nb $3d_{5/2}$ value is different from that for bulk NbS_2[20] and 3R-NbS_2 films (from $NbCl_5$/*t*BuSH). However, the binding energy shifts compare well with those published for a mixed transition metal disul-

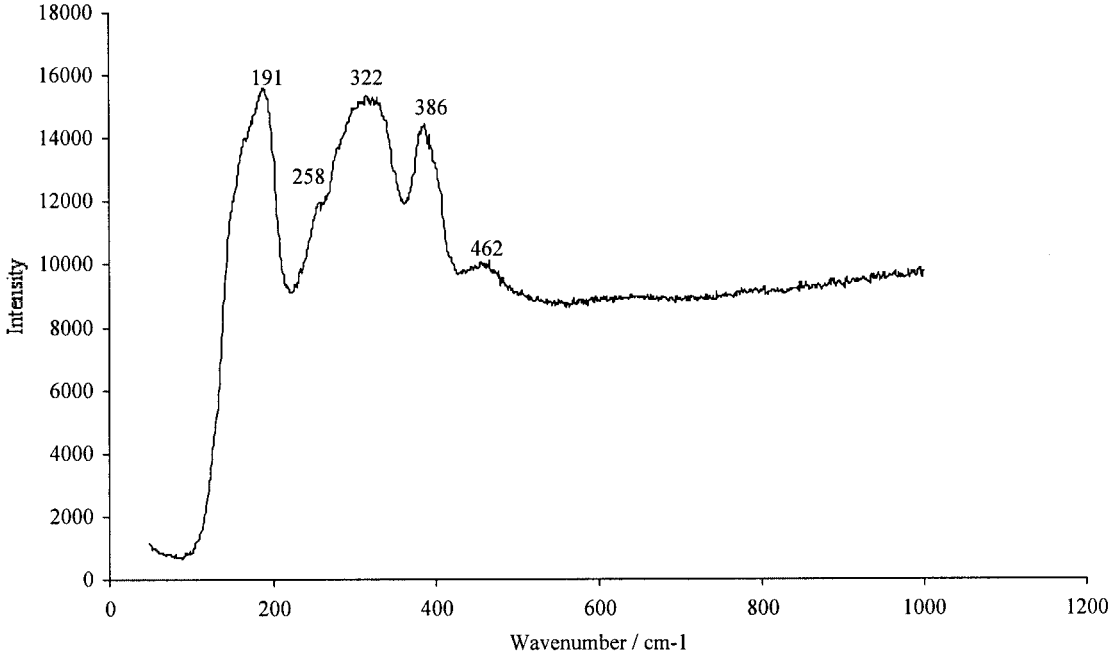

Figure 5. Raman spectrum of a NbS_2 film deposited on glass from $NbCl_5$ and *t*BuSH at 550 °C

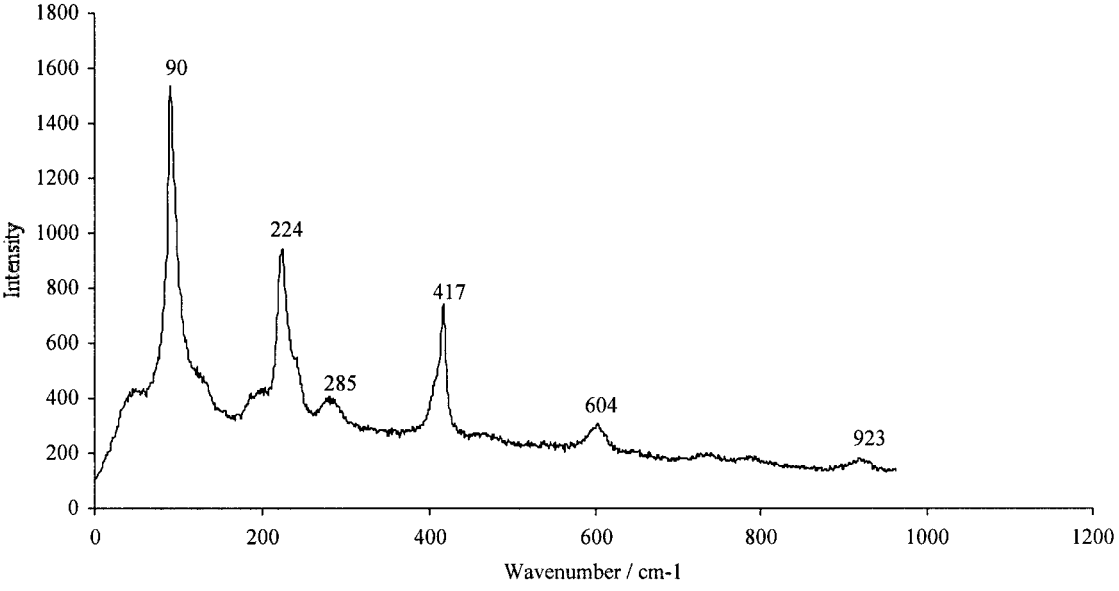

Figure 6. Raman spectrum of a NbS_2 film deposited on glass from $NbCl_5$ and tBu_2S_2 at 550 °C

fide system, 1T-$Nb_{1-x}Ir_xS_2$, which crystallizes into the 1T structure (Nb $3d_{5/2}$ about 206 eV; S 2p 162 eV).[22] These binding energy shifts suggest that the APCVD of $NbCl_5$ and $S(SiMe_3)_2$ or tBu_2S_2 at 500−600 °C results in the formation of a new trigonal polytype 1T-NbS_2, and this is further supported by the powder XRD and Raman spectra for the films.

A wide range of contact angles for water droplets on the NbS_2 films produced were obtained (Table 1). The contact angle measurements are valuable in the glass industry in assessing whether films have self-cleaning properties. Low contact angles arising from hydrophilic films lead to the spreading of the water across the surface, and hence the washing away of any loose dirt. For example, niobium(V) oxide films have been shown to generate low contact angle measurements (about 10°) under photo-irradiation.[23] Some of the niobium sulfide films obtained had contact angles >50° indicating that the films are hydrophobic. However, a number of films had very low contact angles between 2.4° and 14.5° suggesting a degree of hydrophilicity. The contact angles did not change upon photo-irradiation suggesting that this low contact angle is not due to some form of photo-induced hydrophilicity. Thus, the low contact angle is most likely due to a high-porosity within the films. Furthermore, these measurements indicate that the niobium sulfide films are unlikely to be oxide sur-

face terminated since if niobium(v) oxide was present a drop in contact angle on photo-irradiation would be observed.[23] Four-point probe measurements show that the niobium sulfide films are metallic conductors at room temperature, as is expected. Accurate measurements could not be obtained as the films were scratched by the probe, which led to the fluctuation of the reading.

The deposition of NbS_2 films worked best at substrate temperatures between 500 and 600 °C. These results suggest that temperatures in excess of 400 °C are required for the precursors to react completely and form a film. However, nanocrystalline NbS_2 films were obtained from $NbCl_5$ and *t*BuSH at temperatures as low as 350 °C. The lack of chlorine contamination in the resulting films, despite the use of $NbCl_5$ indicates that a clean decomposition pathway is available. This probably occurs via species such as *t*BuCl and Me_3SiCl when tBu_2S_2 and $S(SiMe_3)_2$ are used, respectively. It is also possible that the reactions proceed via the formation of gas phase adducts, for example $[NbCl_5(tBuSH)_x]$.

The calculated growth rate for the formation of 1T-NbS_2 from $NbCl_5/S(SiMe_3)_2$ or tBu_2S_2 at 600 °C is 3.2 μm min^{-1}. This is faster than that for the formation of 3R-NbS_2 from $NbCl_5$/*t*BuSH or $HSCH_2CH_2SH$ at the same growth temperature (0.1 μm min^{-1}). The XPS, Raman, and XRD results suggest that 1T-NbS_2 is the kinetic product ,and this metastable phase forms due to the rapid growth rate. The formation of 1T-NbS_2 when using the sulfur precursors, $S(SiMe_3)_2$ and tBu_2S_2, may also be a result of the faster reaction chemistry relative to *t*BuSH or $HSCH_2CH_2SH$. In addition, it is also possible that $S(SiMe_3)_2$ and tBu_2S_2 do not have low energy decomposition pathways, for example, to yield H_2S, whereas *t*BuSH and $HSCH_2CH_2SH$ could rapidly afford H_2S on thermolysis. However, precursor volatility is also likely to contribute to the phase of NbS_2 obtained. Further studies into the reaction chemistry are required in order to obtain a more definite mechanism for the reaction. The formation of 1T-NbS_2 from $NbCl_5/S(SiMe_3)_2$ or tBu_2S_2 at 600 °C is markedly different from that of $NbSe_2$, where the 1T phase is only stable above 980 °C.[21]

Conclusion

APCVD of $NbCl_5$ and $S(SiMe_3)_2$ or tBu_2S_2 at 500−600 °C form crystalline 1T-NbS_2 thin films on glass. The XRD pattern of these films are not consistent with that of 3R-NbS_2, and appear to have missing reflections when compared with 2H-NbS_2. However, the XRD pattern obtained for the niobium sulfide films compares well with the reported pattern for 1T-TaS_2. The formation of the 1T-NbS_2 phase is further supported by the Raman spectra and XPS data obtained for the films. The dual-source CVD reaction of $NbCl_5$ and *t*BuSH or $HSCH_2CH_2SH$ produced 3R-NbS_2 films. All the films are free from contamination by carbon, oxygen, and chlorine (to detection limits about 0.5 atom%). They show good surface coverage, adhesion, and uniformity.

Experimental Section

Nitrogen (99.99%) was obtained from BOC and used as supplied. $NbCl_5$, $S(SiMe_3)_2$, tBu_2S_2, *t*BuSH, and $HSCH_2CH_2SH$ were supplied by Aldrich and used without further purification. Coatings were obtained on float glass substrates (90 mm × 45 mm × 4 mm) with a ca. 50 nm thick blocking layer of SiCO (to limit diffusion of ions from the glass) on a purpose built reactor.[24] A graphite block containing a Whatman cartridge heater was used to heat the glass substrate. The temperature of the substrate was monitored by a Pt-Rh thermocouple. The rig was designed so that four separate gas lines could be used, all of which were made of 1/4-in. diameter stainless steel, except for the inlet to the reaction chamber and the exhaust line from the reaction chamber which was 1/2-in. diameter. The nitrogen carrier gas was preheated to 157 °C by passing along 2 m lengths of coiled stainless steel tubing inside a tube furnace. Gas temperatures were monitored in situ by Pt-Rh thermocouples. The $NbCl_5$ and sulfur sources were placed into individual bubblers and heated through a heating jacket ($NbCl_5$, 220 °C; $S(SiMe_3)_2$, 90 °C; tBu_2S_2, 170 °C; *t*BuSH, 55 °C; $HSCH_2CH_2SH$, 85 °C). The vapors produced were introduced into a stream of hot nitrogen and transported to the mixing chamber. Flow rates were kept constant for all experiments ($NbCl_5$, 2.0 L·min^{-1}; $S(SiMe_3)_2$, 0.3 L·min^{-1}; tBu_2S_2, 0.3 L·min^{-1}; *t*BuSH, 0.2 L·min^{-1}; $HSCH_2CH_2SH$, 0.2 L·min^{-1}). All systems were investigated over a range of temperatures from the onset of deposition up to 600 °C. The exhaust from the reactor was passed through three bleach bubblers and vented directly into the extraction system of a fume cupboard. Deposition experiments were timed by stopwatch for typically 60 s. At the end of the deposition the bubbler line was closed, and nitrogen was passed over the substrate. The glass substrate was allowed to cool to ca. 60 °C before it was removed. The large substrates were cut into ca. 4 cm × 1 cm strips for analysis by SEM, XPS, Raman, UV/Vis spectroscopy and contact angle studies. 3 cm × 2 cm strips were used for X-ray diffraction. Film adherence to the glass was assessed using the Scotch tape test and by scratching the surface using brass and steel.

X-ray powder diffraction patterns were measured on a Siemens D5000 diffractometer using monochromated Cu-$K_{\alpha 1}$ radiation (λ_1 = 1.5406 Å) with glancing incident radiation (1.5°) or using synchrotron radiation (λ_1 = 1.2982 Å) on beamline 2.3 at the UK Synchrotron Radiation Source. The data contained a large glass background, and this was removed by subtracting a heavily smoothed and normalized data set collected on a glass substrate. Data collected with a copper standard was used to obtain an instrumental Gaussian peak shape, this was then kept fixed when fitting the NbS_2 data. EDXA was obtained with a JEOL 35CF, and SEM was obtained with a Hitachi S570 instrument using the KEVEX system. X-ray photoelectron spectra were recorded with a VG ESCALAB 220i XL instrument using focused (300 μm spot) monochromatic Al-K_α radiation at a pass energy of 20 eV. Scans were acquired with steps of 50 meV. A flood gun was used to control charging, and the binding energies were referenced to an adventitious C 1s peak at 284.8 eV. Depth profile measurements were obtained by using argon beam sputtering. UV/Vis spectra were recorded in the range 190−1100 nm with a Helios double beam instrument. Reflectance and transmission spectra were recorded between 300 and 1200 nm by a Zeiss miniature spectrometer. Reflectance measurements were standardized relative to a rhodium mir-

ror and transmission relative to air. Raman spectra were acquired with a Renishaw Raman System 1000 using a helium-neon laser of wavelength 632.8 nm. The Raman system was calibrated against the emission lines of neon. Contact angle measurements of selected glass samples were determined by measuring the spread of a 7.5 μL droplet of water. Electrical conductivity was determined with a four-probe measurement.

Caution! It should be noted the APCVD reaction of $NbCl_5$ and $S(SiMe_3)_2$, tBu_2S_2, tBuSH or $HSCH_2CH_2SH$ could conceivably produce H_2S. Care should be taken to conduct all experiments in a fume cupboard and pass the exhaust gases through a series of bleach scrubbers.

Acknowledgments

E. S. P. thanks the EPSRC for a studentship. I. P. P. thanks the EPSRC for purchase of the Renishaw Raman microscope (GR/M82592). CCLRC is thanked for beamtime at the SRS at Daresbury (40056). A. L. H. is supported by a Royal Society University Research Fellowship.

[1] P. Lavela, J. Morales, L. Sanchez, J. L. Tirado, *J. Power Sources* **1997**, *68*, 704−707.
[2] Z. -M. Li, B. Bergersen, *J. Phys. C: Solid State Phys.* **1986**, *19*, 7281−7290.
[3] C. Liu, R. F. Frindt, *Phys. Rev. B* **1985**, *31*, 4086−4088.
[4] Z. -M. Li, B. Bergersen, P. Palffy-Muhovay, D. Beigie, *Can. J. Phys.* **1988**, *66*, 228−232.
[5] J. Afonso, M. Breysse, N. Allali, M. Danot, *Catal. Today* **1996**, *28*, 23−30.
[6] W. M. R. Divigalpitiya, R. F. Frindt, S. R. Morrison, *J. Phys. D: Appl. Phys.* **1990**, *23*, 966−970.
[7] F. Jellinek, G. Brauer, H. Müller, *Nature* **1960**, *185*, 376−377.
[8] A. Meerschaut, C. Deudon, *Mater. Res. Bull.* **2001**, *36*, 1721−1727.
[9] W. G. Fisher, M. J. Sienko, *Inorg. Chem.* **1980**, *19*, 39−43.
[10] K. Motizuki, Y. Nishio, M. Shirai, N. Suzuki, *J. Phys. Chem. Solids* **1996**, *57*, 1091−1096.
[11] W. M. R. Divigalpitiya, R. F. Frindt, S. R. Morrison, *J. Phys. D: Appl. Phys.* **1990**, *23*, 966−970.
[12] P. J. McKarns, M. J. Heeg, C. H. Winter, *Inorg. Chem.* **1998**, *37*, 4743−4747.
[13] C. J. Carmalt, C. W. Dinnage, I. P. Parkin, A. J. P. White, D. J. Williams, *Inorg. Chem.* **2002**, *41*, 3668−3672.
[14] A communication of part of this work relating to the preparation of NbS_2 thin-films has appearec, see: C. J. Carmalt, T. D. Manning, I. P. Parkin, E. S. Peters, A. L. Hector, *J. Mater. Chem.* **2004**, *14*, 290−291.
[15] A. Spijkerman, J. L. de Boer, A. Meetsma, G. A. Wiegers, S. van Smaalen, *Phys. Rev. B* **1997**, *56*, 13757−13767.
[16] R. B. von Dreele, A. C. Larson, *GSAS: general structure analysis system* Neutron Scattering Centre, MS-H805, Los Alamos National Laboratory, Los Alamos, NM (**2001**).
[17] GSAS technical manual.
[18] W. G. McMullan, J. C. Irwin, *Solid State Commun.* **1983**, *45*, 557−560.
[19] T. Hirata, F. S. Ohuchi, *Solid State Commun.* **2001**, *117*, 361−364.
[20] G. E. McGuire, G. K. Schweitzer, T. A. Carlson, *Inorg. Chem.* **1973**, *12*, 2450−2453.
[21] F. Kadijk, F. Jellinek, *J. Less-Common Met.* **1971**, *23*, 437−441.
[22] M. Shimakawa, K. Kawachi, S. Nishikawa, K. Hayashi, *J. Solid State Chem.* **1997**, *129*, 242−249.
[23] S. A. O′Neill, I. P. Parkin, A. Mills, N. Elliott, *J. Mater. Chem.* **2003**, *13*, 2952−2956.
[24] C. J. Carmalt, I. P. Parkin, E. S. Peters, *Polyhedron* **2003**, *22*, 1499−1505.

Received April 15, 2004
Early View Article
Published Online September 9, 2004

